

**Laboratory rivers adjust their shape to sediment transport**A. Abramian <sup>1,2,\*</sup>, O. Devauchelle,<sup>1</sup> and E. Lajeunesse <sup>1</sup><sup>1</sup>*Université de Paris, Institut de physique du globe de Paris, CNRS, F-75005 Paris, France*<sup>2</sup>*Sorbonne Université, Institut Jean Le Rond d'Alembert, CNRS, F-75005 Paris, France* (Received 16 April 2020; revised 11 September 2020; accepted 10 October 2020; published 2 November 2020)

An alluvial river builds its own bed with the sediment it transports; its shape thus depends not only on its water discharge but also on the sediment supply. Here we investigate the influence of the latter in laboratory experiments. We find that, as their natural counterpart, laboratory rivers widen to accommodate an increase of sediment supply. By tracking individual particles as they travel downstream, we show that, at equilibrium, the river shapes its channel so that the intensity of sediment transport follows a Boltzmann distribution. This mechanism selects a well-defined width over which the river transports sediment, while the sediment remains virtually idle on its banks. For lack of a comprehensive theory, we represent this behavior with a single-parameter empirical model which accords with our observations.

DOI: [10.1103/PhysRevE.102.053101](https://doi.org/10.1103/PhysRevE.102.053101)**I. INTRODUCTION**

The bed of an alluvial river is made of mobile sediment, such as sand or gravel [1]. Its shape results from the action of water on this granular bed: The flow entrains superficial grains and deposit them further downstream, thus deforming the channel that confines it. With time, this coupling selects the size and shape of the river.

The width of a river typically scales with its water discharge. Specifically, it follows the empirical law of Lacey: It is proportional to the square root of the discharge [2]. At leading order, this relationship indicates that the river bed is near the threshold of motion [3]. Indeed, if we assume that each grain of the bed surface is steady, but about to move, then the river's cross section should form a cosine of prescribed dimensions [4]. Laboratory analogues of rivers conform to this theory, for both turbulent and laminar flows [5,6].

Most rivers, however, carry some sediment, and their bed is therefore above the threshold of motion [7,8]. These “active” rivers are generally wider, shallower, and steeper than predicted by the threshold theory and destabilize into braids beyond a critical sediment load [9,10]. Although water discharge is the prime control on their size, sediment discharge also affects the shape of an alluvial river [11,12].

Yet the role of sediment transport in alluvial rivers remains obscure. Its investigation has proven challenging in the laboratory, because most experiments generate braids, as a result of the unhindered growth of bedforms [13,14]. Some experimenters prevent this instability by adding cohesive sediment [14] or by growing riparian vegetation [15]. How necessary these ingredients are, however, remains a matter of debate [16]. Reitz *et al.* [17] and Delorme *et al.* [18] produced active rivers with moderate sediment supply but focused on the alluvial fan they deposit rather than on their internal dynamics. Ikeda *et al.* [19] also maintained an active single channel in

the laboratory by splitting it into halves with a vertical wall, but they did not measure the sediment discharge.

To investigate sediment transport per se, it is easier to confine the flow in a canal or a pipe [20–24]. This configuration, usually referred to as a “flume” experiment, typically provides a relation between the intensity of the sediment flux and the shear the fluid exerts on the bed,  $\tau$ . It is customary to express this relationship in terms of the Shields parameter, defined as the ratio of the fluid force to the weight of a grain [25]:

$$\theta = \frac{\tau}{(\rho_s - \rho_f)gd_s}. \quad (1)$$

When the fluid force overcomes the weight of the grain, the Shields parameter exceeds its threshold value  $\theta_t$ , and bedload transport starts. It then increases linearly with the excess stress (at least for moderate transport):

$$q_s = q_0 (\theta - \theta_t), \quad (2)$$

where  $q_0$  and  $\theta_t$  depend on the fluid and sediment properties.

At moderate shear stress, the particles move by rolling, sliding, and bouncing, while gravity maintains them close to the bed surface. The layer of entrained grains, or “bedload layer,” is only a few grain-diameters thick [20]. When the shear stress becomes more intense, grains can be suspended in the bulk of the flow [24], where they can diffuse across the stream [26]. Here we focus on bedload transport. In laboratory flumes that transport sediment as bedload, the traveling grains collide with the rough sediment bed underneath [27,28]. Particle tracking shows that these collisions turn their trajectories into random walks across the stream. Collectively, bedload particles thus diffuse from areas where their population is dense toward less crowded ones [29]—much like suspended particles.

For the bed to reach equilibrium, another flux must oppose this diffusive flux. Gravity, which pulls the moving grains toward the channel's center, plays this role in laboratory flumes [30] and most likely in natural rivers [7]. The balance between gravity and diffusion then sets the bed's shape and,

\*anaisabramian@gmail.com

surprisingly, its downstream slope. This statistical equilibrium takes the form of a Boltzmann distribution, according to which the sediment flux  $q_s$  decreases exponentially with the bed elevation  $h$  [30]:

$$\frac{q_s}{\langle q \rangle_g} = \exp\left(-\frac{h - \langle h \rangle_a}{\lambda_B}\right), \quad (3)$$

where  $\langle \cdot \rangle_a$  and  $\langle \cdot \rangle_g$  are the arithmetic and geometric means, respectively, and  $\lambda_B$  is the length that measures the relative importance of diffusion and gravity. To our knowledge, the latter was measured only once experimentally, for plastic grains entrained by a viscous fluid flowing in a flume ( $\lambda_B = 0.12 \pm 0.02 d_s$ , where  $d_s$  is the grain size) [30].

The same mechanism likely occurs in laboratory rivers which, unlike confined flumes, can adjust their width. If so, then it should account for the entire shape, too. To test this hypothesis, we generate single-thread rivers of which we vary the sediment discharge (Sec. II). We then measure the bed elevation and the cross-stream profile of the sediment flux by tracking individual grains (Secs. III and IV). Finally, we observe that this distribution selects the width of a river, which increases with sediment discharge (Sec. VI).

**II. EXPERIMENTAL SETUP**

To generate our laboratory rivers, we use an inclined plane (90 × 190 cm), covered with a 5-cm-thick layer of plastic grains [30] (Fig. 1). All grains have the same density and size (density  $\rho_s = 1490$  g/l; median diameter  $d_s = 0.82 \pm 0.19$  mm), but they come in a variety of colors. We will use the latter to track the traveling grains and measure the sediment flux (Sec. IV).

At the beginning of an experiment, we level the sediment bed with a rake and carve a straight channel into it, from the inlet to the outlet. The initial slope of the sediment bed is about  $10^{-3}$ , but we cannot accurately fix this value. We then inject a mixture of glycerol and water (density  $\rho_f = 1160 \pm 5$  g/l, viscosity  $\nu = 10$  cP). A tank placed above the experimental setup delivers a constant discharge  $Q_w$  in the range 0.1–3 l/min. We measure the density of the fluid every hour and infer its viscosity from this measurement. During a run, we regularly add water to the mixture to compensate for its evaporation. The Reynolds number of the river remains close to 10; the flow is therefore laminar.

We also feed the river with sediment using an industrial feeder (Gericke GLD 87), the screw of which pushes grains into the funnel that guides them toward the inlet. The rotation speed of the screw controls the sediment discharge in the range 0.2–20 g/min. Grains then settle down and concentrate near the bed, as they begin their travel downstream.

During the first hour of a run, the flow spreads over the entire bed, and forms an almost uniform sheet of fluid. Over the next few hours, though, the flow carves a channel, usually along the one we have incised initially. During this transient, the river continuously entrains more grains than it deposits and thus erodes its bed. As a result, the sediment discharge in the channel is larger than the one we impose at the inlet (Fig. 2). Gradually, the sediment flux returns to steady state, until it eventually matches the input  $Q_s$ .

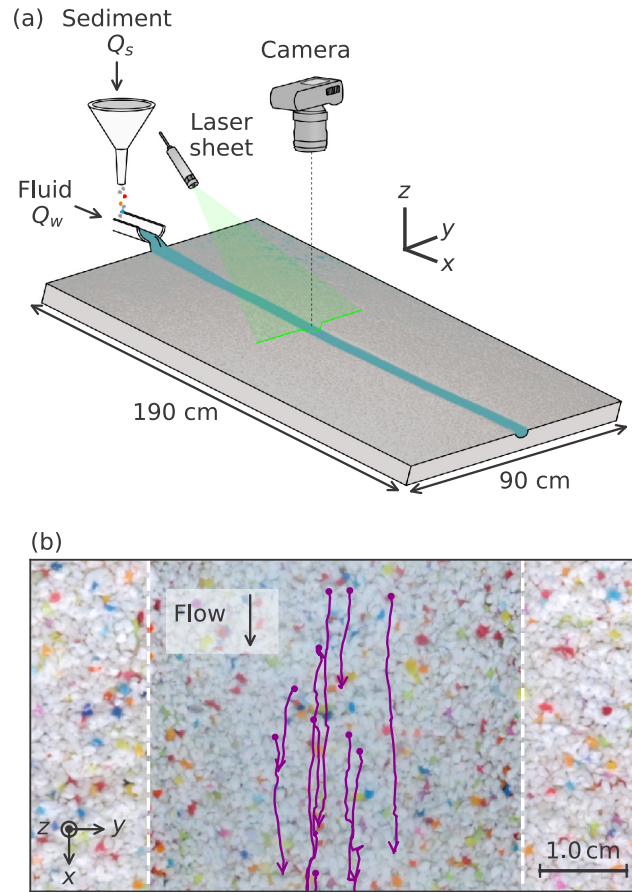


FIG. 1. Experimental setup. (a) Laboratory river, with a top-view camera and inclined laser sheet.  $Q_w$  and  $Q_s$  denote the flow and the sediment discharges, respectively. (b) Close view on the river bed. White dashed lines materialize banks. A few grain trajectories are plotted in pink.

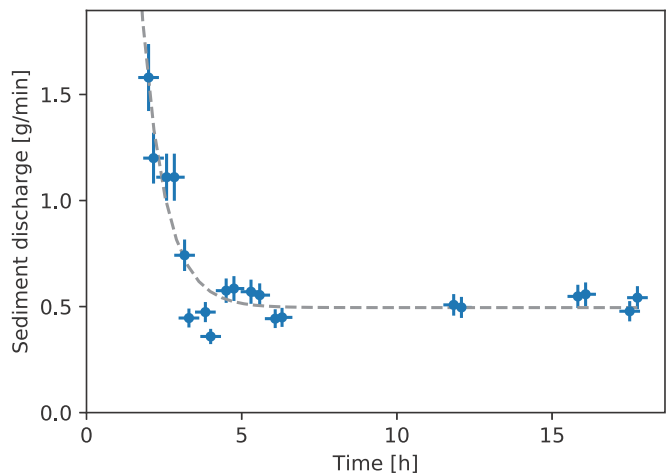


FIG. 2. Evolution of the sediment discharge in a laboratory river. Blue dots: Sediment discharge measured with particle tracking (10-min average). Dashed line: Exponential relaxation with 45-min time constant (fitted to data). Sediment supply is  $0.6 \pm 0.1$  g/min.

TABLE I. Experimental parameters.

Run label	Sediment supply (g min <sup>-1</sup> )	Fluid input (l min <sup>-1</sup> )	Tracking duration (min)	Number of trajectories longer than 4 $d_s$
1	0	1.00	—	—
2	0.78	0.99	72	15 332
3	0.42	1.00	144	10 538
4	0.22	0.87	177	8177
5	1.04	0.98	108	29 696

At equilibrium, the flow forms a straight, single-thread channel, a few centimetres wide [Fig. 1(b)]. This equilibrium is dynamical: Grains are constantly dislodged from the bed, while new ones get deposited by the flow. On average, the sediment discharge is constant, and the river bed does not change much. Moving grains, however, indicate that the bed remains above the threshold of entrainment, in contrast with rivers that are not fed with sediment [5].

At the beginning of each experiment, we set the slope of the frame. However, the layer of sediment is thick enough for the river to later adjust its own slope. The slope is thus chosen by the system and not a control parameter. If the frame's slope is too steep, then the river incises a gorge into the sediment bed, until it reaches its equilibrium slope. Conversely, if the frame's slope is too shallow, then the river deposits its load near the inlet, where the sediment accumulates into an alluvial fan [18]. To hasten the transient, we adjust the frame's slope to match equilibrium. This procedure largely relies on the experimenter's intuition.

Beyond a sediment supply of about 1.5 g/min, the river destabilizes into a braid of intertwined, active channels. This instability, which tightly bounds the sediment supply in our experiments, might explain why active single-thread rivers are so sparse in the literature [6,32]. Its origin remains debated [33,34], and this question would require a dedicated investigation.

Overall, the equilibrium shape of our single-thread rivers depends on two inputs, the fluid and the sediment discharges. To investigate the influence of the latter on the river's shape, we perform a series of experimental runs with the same fluid discharge (about 1 l/min) but for different values of the sediment supply (Table I).

### III. CROSS SECTION

After the river has reached steady state, we measure its cross section with an inclined laser sheet projected onto its bed (Fig. 1). We first locate the laser line, whose position is shifted by the fluid. Then we stop the fluid and sediment inputs and let the fluid drain out of the channel. The traveling grains settle down within a few seconds, and the bed's surface appears to freeze. After the fluid has drained out, we detect the location of the laser line on the bare surface of the bed. The combination of the two laser lines, with and without fluid, provide us with the bed elevation and the flow depth  $D$  within an accuracy  $\delta D = 0.5$  mm, which is slightly less than a grain diameter (see Addendum for details).

Figure 3 shows the cross section of three laboratory rivers. For a vanishing sediment supply, the river's cross section looks rounded [Fig. 3(a)]. This feature accords with the observations of Seizilles *et al.* [5], who interpreted them in terms of the threshold theory. According to this theory, a river that transport no sediment maintains its bed at the threshold of motion. Its cross section should then be [5]

$$D(y) = D_0 \cos\left(\frac{yS_0}{L}\right), \quad (4)$$

where  $D_0$  is the maximum depth of the river and  $S_0$  its downstream slope.  $L$  is a characteristic length depending on the properties of the sediment and the fluid. It reads:

$$L = \frac{\theta_t (\rho_s - \rho_f) d_s}{\mu_t \rho_f}, \quad (5)$$

where  $\mu_t$  is the friction coefficient of the grains and  $\theta_t$  is their threshold Shields number. The threshold theory prescribes not only the river's shape but also its downstream slope, which depends on the fluid discharge  $Q_w$ :

$$S_0 = \left(\frac{4g\mu_t^3 L^4}{9\nu Q_w}\right)^{1/3}. \quad (6)$$

Likewise, the depth of the threshold river depends on its fluid discharge through

$$D_0 = \frac{\mu_t L}{S_0}. \quad (7)$$

In the absence of sediment supply, our experimental river accords with this threshold theory, without fitting any parameter [Fig. 3(a), dashed line with  $L = 0.06 d_s$  and  $S_0 = 0.0046$ ].

More intriguingly, when the sediment supply increases, the river widens and shallows [Figs. 3(c) and 3(e)]. A sediment supply of 1 g/min, for instance, doubles the aspect ratio of the river. The flat cross section of these active laboratory rivers resembles that of a natural river—more so than the rounded shape of Fig. 3(a) [7]. As they adjust to the sediment supply, our laboratory rivers thus adopt a more realistic shape.

When setting up a new experimental run, we need to manually adjust the inclination of the frame to match the expected slope of the river. As the sediment input increases, we need to steepen the frame more and more. This observation suggests that the equilibrium slope of our rivers increases with sediment discharge, in accordance with previous measurements [18,35]. Unfortunately, the river slope, of the order of 0.005 in our experiments, induces a change of bed elevation of the order of 5 mm per meter of river, a value far below the detection range of our experimental setup.

In the next section, instead, we focus on the mechanism by which a river adjusts its cross section.

### IV. SEDIMENT-FLUX PROFILE

Based on previous observations in confined canals [30], we suspect that the balance between bedload diffusion and gravity sets the shape of our rivers. To test this hypothesis, we first need to measure the local sediment flux  $q_s$ . To do so, we track individual grains entrained by the flow using the method described in Abramian *et al.* [30]. With the top-view camera, we first record a 1 h-long movie of the grains traveling over

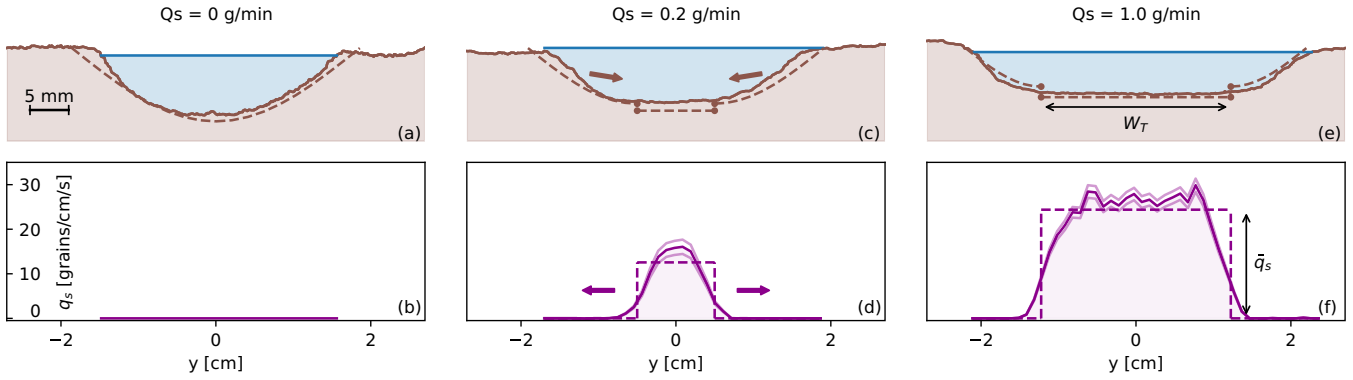


FIG. 3. Bed elevation and sediment-flux profile for runs 1, 4, and 5 (sediment supply increases from left to right). (a) River bed in the absence of sediment supply. Dashed line: Cosine shape predicted by the threshold theory for  $L = 0.06 d_s$  and  $S = 0.0046$  [Eq. (4)]. [(c) and (e)] River beds with sediment supply. Dashed line: Theory of Sec. VI. [(b), (d), and (f)] Experimental sediment-flux profiles. Dashed line: Empirical model of Sec. VI. Brown arrows in (c) and purple arrows in (d) illustrate gravity and diffusion sediment fluxes, respectively. Data are available in the supplemental material [31].

the bed surface (50 fps, see the movie in the supplemental material [31]). We then track independently the motion of the blue, red, and orange grains, based on their color [Fig. 4(a)], and reconstruct their trajectories [Table I, Fig. 1(b)].

For each run, and for each grain color, we then calculate the cross-stream profile of the sediment flux. To account for the proportion of each color in the sediment, we normalize each profile so that its integral matches the sediment input  $Q_s$ .

The three independent measurements are consistent [Fig. 4(b)], with a variability of less than about 15% [Fig. 4(b)]. The uncertainty about their average depends on the number of trajectories but remains below 5% [30].

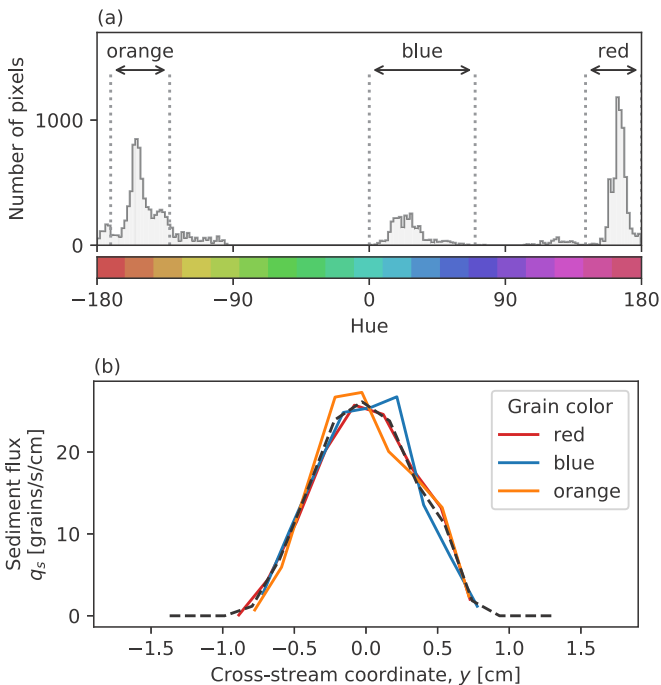


FIG. 4. (a) Histogram of pixel hue in a single frame for run 3. (b) Sediment-flux profile for different grain colors (red, blue, and orange). Dashed black line: Average.

Repeating this procedure with different experimental runs, we find that the shape of the sediment-flux profile varies with  $Q_s$  [Figs. 3(d) and 3(f)]. Its maximum, always near the center of the channel, increases with the total sediment discharge, meaning that bedload transport intensifies. For a high sediment discharge, it is almost uniform in the center of the channel, where the bed is virtually flat [Fig. 3(f)]. Bedload transport then quickly vanishes near the banks.

Equation (2) provides an estimate for the Shields parameter in our rivers, based on the sediment flux. We find that the latter exceeds its threshold value by less than  $0.3 \theta_t$ , indicating that our rivers stay well within the linear regime of the transport law. In other words, our experimental rivers select their shape such that the shear stress remains close to its critical value—another instance of self-organized criticality, at least in the loose sense of a system that spontaneously approaches its critical point [36].

## V. BOLTZMANN EQUILIBRIUM

In our laboratory rivers, like in a flume, the sediment-flux profile and the bed's shape adjust to the sediment discharge. Following Abramian *et al.* [30], we now test whether this adjustment brings the sediment flux to the Boltzmann equilibrium, as expressed by equation (3). To do so, we plot the bed elevation with respect to its own arithmetic mean  $\langle h \rangle_a$ , as a function of the sediment flux, divided by its geometric mean  $\langle q_s \rangle_g$  [Fig. 5(b)]. We find that, regardless of the sediment discharge, the data points gather around the same line in the semilogarithmic space. The profiles being symmetric, they trace this line twice for each river. The slope of each line is comparable to the one measured in a confined flume [30] [black dashed line, Fig. 5(b)].

This observation shows that, in a laminar river, sediment transport converges to the same statistical equilibrium as in a confined flume. This equilibrium sets both the cross section of the bed, and the sediment-flux profile. In addition, laboratory rivers adjust their width. We interpret this adjustment as follows: As Parker [7] first noted, gravity pulls the traveling grains toward the center of the channel and thus tends to

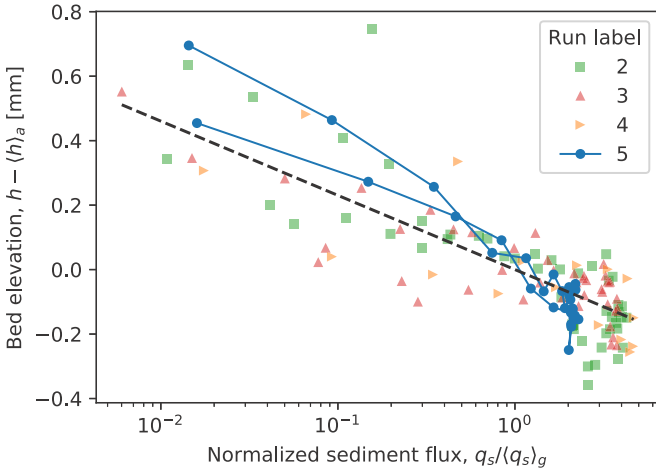


FIG. 5. Boltzmann distribution in our rivers. Colors correspond to runs (Table I). Black line shows Eq. (3) without fitting parameter ( $\lambda_B = 0.12 d_s$  after Ref. [30]).

widen the river. Bedload diffusion counters this widening by pushing grains toward the banks, where transport is weaker. The resulting balance sets the equilibrium shape of the river.

Despite its simplicity, however, the mathematics of this coupling remains elusive. Most of the difficulty lies in the fluid flow, of which the lubrication approximation provides only a poor representation [34,35]. Below, instead, we propose a semiempirical model that, hopefully, delineates the problem.

### VI. RIVER BED MODEL

Figure 5 shows that our laboratory rivers adjust their shape so that diffusion and gravity can balance each other. We now wish to relate this grain-scale mechanism to the morphology of the river: its width, its aspect ratio, and its slope.

Boltzmann statistics provides a relation between the sediment flux and the river depth. In addition, the sediment flux is related to the flow-induced shear stress through the transport law. To close this system of equations, we need an additional relation: The momentum balance that yields the flow-induced force that moves the grains. In other words, we need to compute the flow in the river. This is not an easy task, though: As we do not know the shape of the river *a priori*, we need to solve a two-dimensional, free-boundary problem.

The simplest way to bypass this problem is to invoke the lubrication approximation [[35], chap. 4]. In this framework, one assumes that the shear stress  $\tau$  is simply proportional to the flow depth:

$$\tau = \rho g D S. \tag{8}$$

Supplemented with Boltzmann statistics and the transport law, this expression yields a first-order, ordinary differential equation for the flow depth. This equation reproduces qualitatively our experimental observations—for example, the fact that a river widens as it transports more sediment [[35], chap. 4]. However, it overestimates the increase of the width by a factor of more than 3. We suspect that this discrepancy results from the lubrication approximation. Indeed, it can only provide a rough estimate of the shear stress, and therefore of the Shields

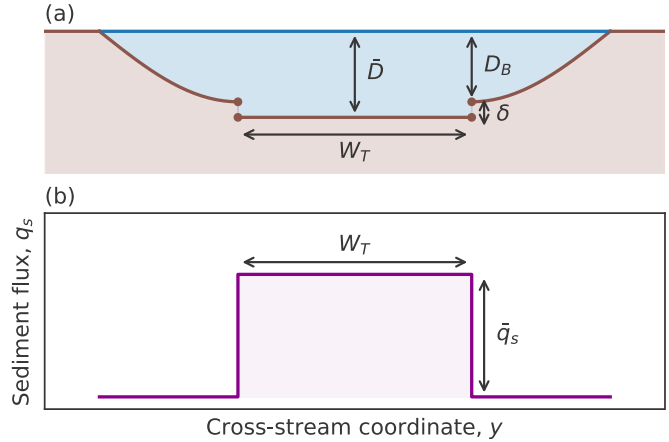


FIG. 6. Model of an active river (Sec. VI). (a) Cross section. Blue: River flow. Brown: Sediment bed. (b) Sediment-flux profile.

parameter  $\theta$ . Since the river is near the threshold ( $\theta \approx \theta_t$ ), the transport law (2) amplifies the slightest error on the shear stress into a major change of the river’s shape [[35], chap. 4].

For lack of a better theory, we propose here a simpler, semiempirical model which eschews the complete calculation of the fluid flow. Inspired by the cross sections of Fig. 3, and by previous work [7,37], we decompose the cross section of a river into three parts: the central part, which we assume to be flat, and the two banks that bound it [Fig. 6(a)]. We consider the central part as an active segment of width  $W_T$ , where the river uniformly transports sediment [Fig. 6(b)].

On this active segment, we replace the depth, the sediment flux, or any other quantity  $f$  by its average  $\bar{f}$ , weighted by the local intensity of sediment transport:

$$\bar{f} = \frac{1}{Q_s} \int_{-\infty}^{+\infty} f q_s dy. \tag{9}$$

The limits of the above integral are infinite in principle, but they reduce to the river’s width in practice. This average, devised with the Boltzmann equilibrium in mind, differs from the ensemble means denoted with brackets in Sec. V. Whereas the latter gives equal weight to every measurement point, the average of Eq. (9) winnows the active section of the river from its steady parts, the banks.

Finally, we assume that the banks are at the threshold of motion, and therefore approximate their shape with a cosine (restricted to a quarter of its period). These banks, however, adjust their downstream slope to that of the active segment. We also allow them to adjust their size accordingly. In other words, we assume that each bank is half a threshold river, with a slope that matches that of the total river.

In the next section, we relate the parameters of this model (the slope, width, and depth of the river), to the sediment and water discharges. To do so, we first establish an empirical relationship between the transport width and the sediment discharge. Using the transport law (2), we then estimate the slope of the river and its entire cross section.

### A. Sediment transport

In the simple model sketched above, the sediment-flux profile is a rectangle, of width  $W_T$  and height  $\bar{q}_s$ , where  $\bar{q}_s$  is the average intensity of sediment transport, defined by equation (9) [Fig. 6(b)]. To estimate the transport width, we require the area of this rectangle to be the sediment discharge  $Q_s$ , that is,

$$W_T = \frac{Q_s}{\bar{q}_s}. \quad (10)$$

We also assume that  $W_T$  vanishes with  $Q_s$ , that is, in a river exactly at threshold.

A convenient feature of the average defined by Eq. (9) is that it is based on our most reliable measurement: the sediment-flux profile. This makes quantities such as  $\bar{q}_s$  and  $W_T$  experimentally robust. We find that the simplified sediment profile they define resemble the original [Figs. 3(d) and 3(f), dashed lines].

Following Seizilles *et al.* [5], we normalize the intensity of sediment transport with  $\theta_t/\mu_t q_0$ , where  $q_0$  is the prefactor of the transport law [Eq. (2)]. For our grains and fluid,  $q_0 = 544 \pm 48$  grains/cm/s and  $\theta_t = 0.167 \pm 0.003$  [30]. Similarly, we define for later convenience the characteristic sediment discharge  $Q_s^*$  as [18]:

$$Q_s^* = d_s \frac{\theta_t q_0}{\mu_t}, \quad (11)$$

Physically,  $Q_s^*$  can be interpreted as the characteristic discharge of grains across a segment of one grain size. This quantity depends on the fluid and sediment properties only, which we did not vary in our experiments. It is  $9.5 \pm 1.5$  grains/s. Finally, in accordance with the above choices, we normalize the width  $W_T$  by the grain size  $d_s$ .

We now plot  $W_T$  and  $\bar{q}_s$  as functions of the sediment discharge [Figs. 7(a) and 7(b)]. As expected, these two quantities increase with the sediment discharge of the river. By fitting power laws on these observations, we find:

$$\frac{W_T}{d_s} \propto \left(\frac{Q_s}{Q_s^*}\right)^\alpha \quad \text{and} \quad \frac{\bar{q}_s d_s}{Q_s^*} \propto \left(\frac{Q_s}{Q_s^*}\right)^\beta \quad (12)$$

with  $\alpha = 0.6 \pm 0.1$  and  $\beta = 0.4 \pm 0.1$ . As the two exponents are about 0.5, we expect the active width  $W_T$  to be proportional to the intensity of sediment transport  $\bar{q}_s$ . If so, the rectangle that represents the sediment flux in our model should preserve its aspect ratio as the sediment discharge varies [Figs. 3(d) and 3(f)]. To check this, we plot the rectangle's height as a function of its width, and find that the linear relation

$$\frac{\bar{q}_s d_s}{Q_s^*} = c_T \frac{W_T}{d_s} \quad (13)$$

fits our data best for  $c_T = (8.5 \pm 0.9) \times 10^{-3}$  [Fig. 7(c)]. We expect that the value of this parameter depends on the water discharge, which we did not vary in our experiments.

For simplicity, we now assume that the exponents  $\alpha$  and  $\beta$  are exactly 0.5, that is [dashed lines, Figs. 7(a) and 7(b)]:

$$\frac{\bar{q}_s d_s}{Q_s^*} = \sqrt{c_T \frac{Q_s}{Q_s^*}} \quad \text{and} \quad \frac{W_T}{d_s} = \sqrt{\frac{1}{c_T} \frac{Q_s}{Q_s^*}}. \quad (14)$$

This assumption enables us to estimate the active width of a river, based on its sediment discharge  $Q_s$  only. We do not know

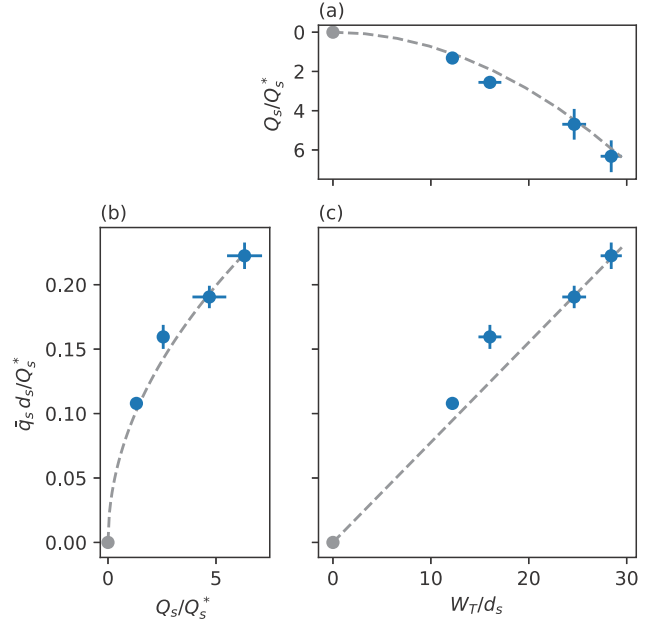


FIG. 7. Average intensity and width of the sediment-flux profiles. (a) Active width of the channel  $W_T$  as a function of the sediment discharge. Blue points: Experimental rivers. Dashed line: Equation (14) fitted to data. (b) Average sediment flux  $\bar{q}_s$  as a function of sediment discharge. Blue points: experimental rivers. Dashed line: Equation (14) fitted to data. (c) Average intensity of the profile as a function of the active width of the channel. Blue points: Experimental rivers. Dashed line: Equation (13) fitted to data.

the physical origin of this relation. In the following, we use it as an empirical result and investigate how it sets the river's cross section.

### B. Cross section and slope

Once we know the active width of a river,  $W_T$ , and the average intensity of sediment transport,  $\bar{q}_s$ , we can calculate the average depth  $\bar{D}$  of the active segment based on the transport law (2). We first invoke the shallow-water approximation, which translates mathematically into the shear stress being proportional to  $\bar{D}$ . Expressed in terms of the Shields parameter, this proportionality reads

$$\bar{\theta} = \frac{\rho_f \bar{D} S}{(\rho_s - \rho_f) d_s}. \quad (15)$$

Introducing this expression in Eq. (2) and replacing  $\bar{q}_s$  with Eq. (14), we get the depth of the active segment,

$$\frac{\bar{D}}{D_0} = \frac{S_0}{S} \left(1 + \frac{1}{\mu_t} \sqrt{c_T \frac{Q_s}{Q_s^*}}\right), \quad (16)$$

where  $S_0$  and  $D_0$  are the slope and the depth of the threshold channel that conveys the same fluid discharge [Eqs. (6) and (7)]. By definition, these quantities do not depend on the sediment discharge. Instead, they encapsulate the dependence of the river's cross section on the fluid discharge. In Eq. (16),

however, the actual slope  $S$  of the river is still unknown, and, most likely, depends on the sediment supply. To calculate this slope, we first write the fluid discharge as the sum of the discharge associated to the active segment, with that associated to the banks:

$$Q_w = U\bar{D}W_T + \int_{\text{banks}} U D dy. \quad (17)$$

To calculate the first term, we replace  $W_T$  with Eq. (14),  $\bar{D}$  with Eq. (16), and invoke the lubrication approximation, according to which the vertical velocity profile is that of a Poiseuille flow, namely,

$$U = \frac{g\bar{D}^2 S}{3\nu}. \quad (18)$$

The error induced by the shallow-water approximation is far less critical for the discharge than for the shear stress.

The second term is the contribution of the banks, which are at the threshold of entrainment. Their shape therefore obeys Eq. (4), where we replace the threshold slope  $S_0$  by the slope  $S$  of the active segment, that is, the slope of the river. The downstream slope at the banks thus matches that of the active segment. Following this assumption, we get:

$$D = D_B \cos\left(\frac{yS}{L}\right), \quad \text{with } D_B = \frac{S_0 D_0}{S}. \quad (19)$$

Equation (19) sets the depth  $D_B$ , and the width  $\pi L/S$ , of the banks. Both are proportional to the inverse of the slope and thus decrease with with the sediment discharge. Finally, Eq. (19) allows us to calculate the contribution of the banks to the water discharge in Eq. (17), using the lubrication approximation again [Eq. (18)].

We finally combine Eqs. (16), (17), and (19) to relate the river's slope to its water and sediment discharges. In the resulting expression, the slope  $S$  depends on  $Q_s$  and  $Q_w$  implicitly:

$$\left(\frac{S}{S_0}\right)^3 = \left[1 + \frac{3}{4} \frac{d_s S}{L} \sqrt{\frac{1}{c_T} \frac{Q_s}{Q_s^*}} \left(1 + \frac{1}{\mu_t} \sqrt{c_T \frac{Q_s}{Q_s^*}}\right)^3\right] \frac{Q_w}{Q_w^*}. \quad (20)$$

According to the above equation, the slope increases with  $Q_s$ , in agreement with our qualitative observation [Fig. 8(a)]. Unfortunately, this slope is too small for us to measure it in our experiments. Nevertheless, Delorme *et al.* [18] observed a trend that accords with Eq. (20), although for different grains in a more viscous fluid.

Using Eq. (20), we can now determine the entire cross section of our rivers. We find a good qualitative agreement between the empirical model and our experimental profiles [Figs. 3(c) and 3(e), dashed lines]. In Sec. VID, we quantitatively compare the river's width and depth to the present model. Before that, however, we detail how the banks connect with the active segment.

### C. Junction with the banks

The model exposed in the previous sections implicitly assumes that the profile is discontinuous at the junction between the banks and the active segment, with a gap of amplitude  $\delta = \bar{D} - D_B$  [Fig. 6(a)]. This unrealistic feature results from

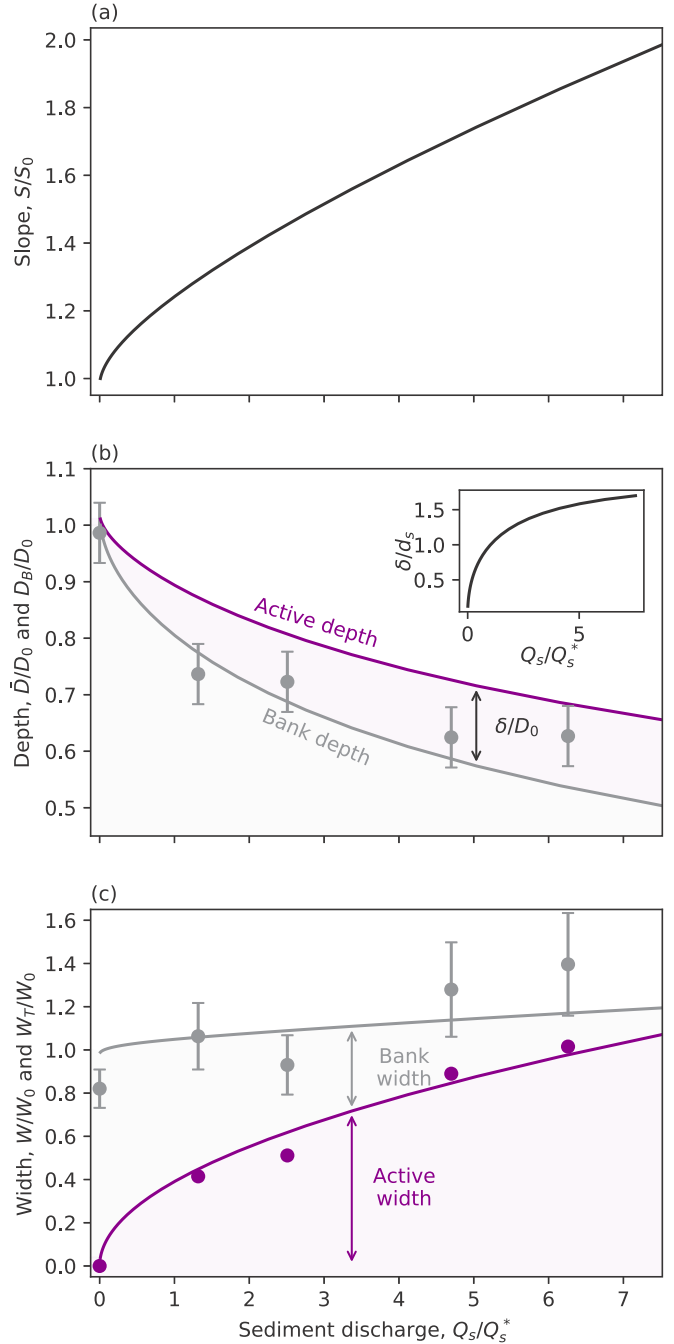


FIG. 8. Width and depth of laboratory rivers. (a) Slope as a function of sediment discharge [Eq. (20)]. (b) Depth as a function of sediment discharge. Gray line: Banks depth  $D_B$  [Eq. (19)]. Pink line: Transport depth  $\bar{D}$  [Eq. (21)]. Points: Experiments. Inset: Discontinuity  $\delta$  as a function of the sediment discharge [Eq. (22)]. (c) Width as a function of sediment discharge. Gray line: Total width predicted by the model of Sec. VI. Gray points: Experimental width. Pink line: active width [Eq. (14)]. Purple points: Experimental active widths.

our inability to evaluate the continuous variation of the shear stress along the river bed. Of course, there is no discontinuity in our experiments, but the above definition of  $\delta$  still holds. In practice, it corresponds to a gradual change of depth across the river, of which the theoretical discontinuity is but a rough

representation. Using the above definition, Eq. (16) reads:

$$\bar{D} = D_B \left( 1 + \frac{\delta}{D_B} \right) \quad (21)$$

with

$$\frac{\delta}{D_B} = \frac{1}{\mu_t} \sqrt{c_T \frac{Q_s}{Q_s^*}}. \quad (22)$$

When the sediment discharge vanishes, the difference of depth between the bank and the river's center vanishes as well ( $\delta = 0$ ). After equation (22), it increases with  $Q_s$ , and should reach about  $1.5 d_s$  at most in our experiments [Fig. 8(b), inset]. Unfortunately, we cannot test this equation directly in our experiment, because we cannot measure the banks depth,  $D_B$ , with decent accuracy. To do so, one would need to fit a cosine to the banks—a procedure far too unreliable for our noisy profiles. Instead, in the next section, we turn to the depth and width of our laboratory rivers.

#### D. Comparison with experiments

Apart from their discontinuity at the banks, the approximate cross sections we propose look like those of our laboratory rivers [Figs. 3(c) and 3(e), dashed lines].

To confirm this impression, we compare the depth of our experiments with their estimate. In our experiments, the transport depth  $\bar{D}$  is indistinguishable from the bank depth  $D_B$ . The former, being averaged over the cross section, is measured with a better precision than the latter. It is therefore the measured value of  $\bar{D}$  that we compare to the theoretical estimates provided by Eqs. (19) and (21) [Fig. 8(b)]. We find that most data points lie between  $D_B$  and  $\bar{D}$ . Within the uncertainty of our measurements (about  $5 d_s$ , Sec. III), the experiments thus conform to our semiempirical theory.

We now turn our attention to the width of our experimental rivers. The most intuitive way to measure this quantity is to locate the points where the river depth vanishes. In practice, however, this method is sensitive to measurement noise. To reduce the latter, we prefer to define the width  $W$  of a river as the ratio of its cross-section area to the transport depth  $\bar{D}$ , such that:

$$W = \frac{1}{\bar{D}} \int D dy \quad (23)$$

(this width is distinct from the active width,  $W_T$ , defined in Sec. VIA: It includes that of the banks). We then rescale  $W_T$  with respect to that of the threshold channel,  $W_0$ , and plot it as a function of the sediment discharge [dashed gray line, Fig. 8(c)]. This ratio is 1 for a vanishing sediment discharge, and increases with sediment discharge, in accordance with our observations [gray points, Fig. 8(c)]. Within the range of sediment discharge explored in our experiments, the width of the river only increases by about 20%.

Equation (23) has the advantage of being linear with respect to the depth profile. Returning to the model of Sec. VIA, this allows us to decompose the total width of a river into the sum of the transport width and the width of the banks

[Fig. 8(c)], that is:

$$W = W_T + \frac{2L}{S}. \quad (24)$$

Based on this decomposition, we propose the following interpretation of a river's adjustment to sediment transport. When a river transports more sediment, its active segment widens, and shallows. The banks adjust their depth to this shallowing, and, their aspect ratio being constant, also narrow as the sediment discharge increases. As a result, the total width of the river depends only weakly on the sediment discharge: the narrowing of the banks counters the widening of the active part. Accordingly, the total width of our laboratory rivers barely varies with their sediment discharge [Fig. 8(c)].

## VII. CONCLUSION

At first order, active laboratory rivers adjust the shape of their bed so that the flow-induced shear stress remains close to the threshold of sediment transport. In nature, the shear stress on the bed of a river seldom exceeds the threshold by more than 10%, suggesting that natural rivers adjust their cross section in a similar fashion [38].

The cross section and the sediment flux of our laboratory rivers organize themselves into a Boltzmann distribution of which only the partition function depends on the sediment discharge. We interpret this observation as the macroscopic signature of the balance between cross-stream diffusion and gravity [30]. We believe that this statistical equilibrium controls the shape of the river, but we do not, at this point, understand how this happens.

Anyhow, we find that, in our experiments, a river accommodates a larger sediment discharge by widening its center, where transport occurs, while narrowing its banks. These two adjustments counteract each other, resulting in a weak variation of the total width of the river. If this trend holds in the field, then the width of a river is not a good proxy for its sediment discharge. We suggest that the aspect ratio is a better one, because the shallowing and the widening of the river conspire to amplify its response to sediment transport. In our experiments, the aspect ratio of the river increases by a factor 2.5 over the range of sediment discharge we have investigated (Fig. 9).

Although the experiments presented here unambiguously show that the river maintains the statistical equilibrium of sediment transport, the process by which this translates into its morphology still eludes us. How the Boltzmann statistics sets the river's cross section, and therefore its aspect ratio, remains an open question. As a first step, we propose here a simple model, based on geometrical arguments, which reduces the problem to a single empirical relation: The transport width is proportional to the square root of the sediment discharge.

The discontinuous model we built upon this observation is at odds with the Boltzmann distribution of the traveling grains, according to which the intensity of sediment transport decreases continuously toward the banks. If the two are to be reconciled, then we will need to estimate more accurately the shear stress the flow exerts on the river bed. This could be improved by taking into account two-dimensional effects in the flow—the purpose of current research.

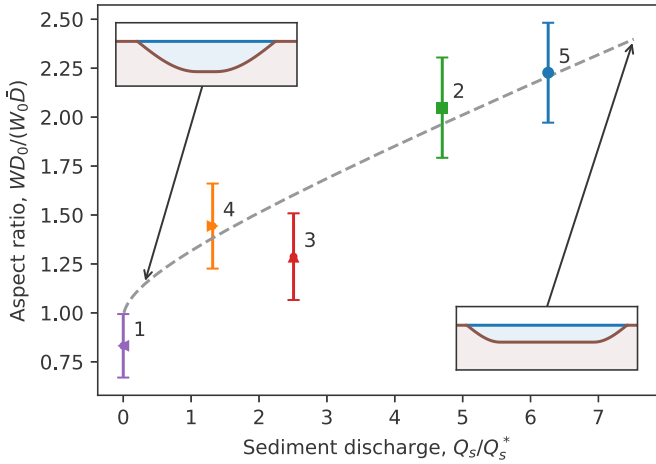


FIG. 9. Aspect ratio of laboratory rivers as a function of their sediment discharge. Each point corresponds to an experimental run, for which we divide the total width of each river [Eq. (23)], by its depth. Colors are those of Fig. 5. Numbers correspond to experimental runs. Dashed line: Prediction of the model developed in Sec. VI.

ACKNOWLEDGMENTS

We thank S. Courrech du Pont, P. Delorme, P. Gondret, and F. M etivier for fruitful discussions. A.A. was partially funded by the Fondation des Treilles.

ADDENDUM

To measure the cross section of our laboratory rivers, we project a laser sheet on the bed’s surface and infer the shape of the latter based on its deviation. Doing so in an active channel, and then in a drained-out one, provides us with the two independent measurements we need to calculate the elevations of the bed and of the water surface.

Pictures from a camera placed above the channel show the intersection of the laser sheet with the bed’s surface (Canon 700 D). As we do not know the inclination  $\phi_{\text{laser}}$  of the laser sheet accurately, we first calibrate this setting by holding aluminium stairs in the field of view of the camera [the shape of this machined piece is known accurately: Each step is 1.0 cm wide and 2.0 mm high, Fig. 10(a)]. After locating the laser sheet’s projection onto each step [Fig. 10(b), green line], we relate it to the stairs’ elevation  $h$ . The coefficient of this linear

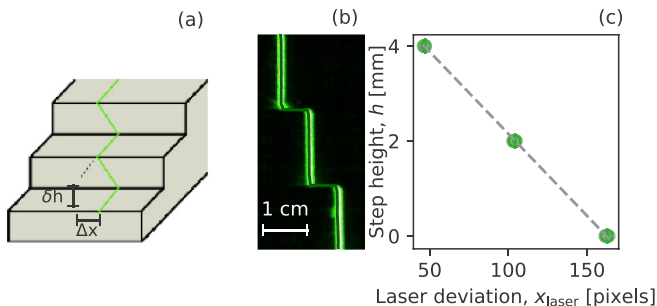


FIG. 10. Calibration of the bed-elevation measurement. (a) Laser sheet on calibrated stairs. (b) Laser line on the stairs (green) and its numerically found location (green line). (c) Linear relation between the height of a step and the corresponding laser deviation [Eq. (25)].

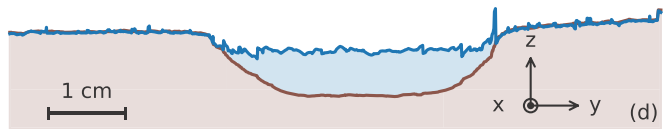
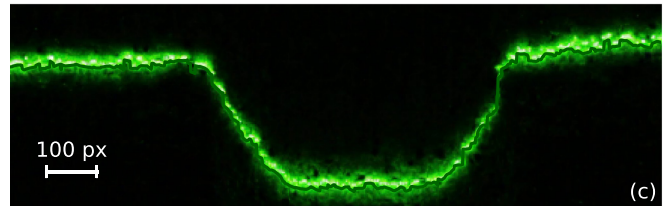
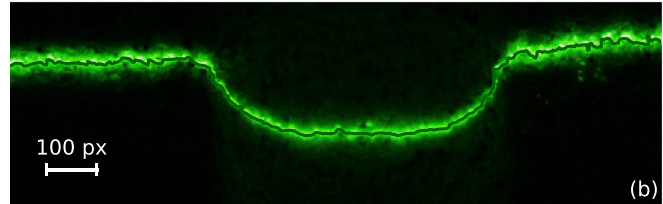
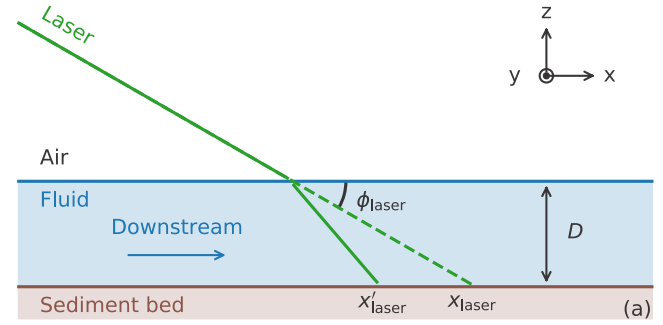


FIG. 11. Measurement of bed elevation and water depth. (a) Side view of the laser sheet projected onto the river bed. Flow from left to right. When the channel is bare, the laser line is located on  $x_{\text{laser}}$ . When it is filled with fluid, the laser is deviated to  $x'_{\text{laser}}$  by the air-liquid interface. (b) Location of the laser line while the bed is filled with fluid (green line). (c) Location of the laser line on a bare bed (green line). (d) Cross section. Brown: Sediment bed. Blue: Fluid.

relation is the tangent of the laser angle:

$$h = \tan \phi_{\text{laser}} x_{\text{laser}}. \tag{25}$$

For the run of Fig. 10, we find  $\phi_{\text{laser}} = 27.54^\circ \pm 0.02^\circ$ .

We then remove the stairs to let the laser intersect the channel’s bed. As the channel is filled with fluid, refraction deviates the laser line to the position  $x'_{\text{laser}}$  [Figs. 11(a) and 11(b)]. The laser line flickers as transported grains cross it. To mitigate these fluctuations, we record a short movie with the top-view camera, and average the resulting images over a few seconds. We then locate the laser line with image analysis [Fig. 11(b), green line].

At this point, we still have only one measurement ( $x'_{\text{laser}}$ ), and two unknown quantities ( $h$  and the water depth). We thus switch off the flow and stop the sediment feeder. As a result, traveling grains settle within a few seconds, while water slowly drains out of the channel. Now, the laser line intersects the bare river bed at  $x_{\text{laser}}$  [Figs. 11(a) and 11(c)], from which

we calculate the bed elevation  $h$  using Eq. (25). In practice, we spatially average the bed elevation by scanning the channel over about one centimetre streamwise (the channel curves too much to average the cross section over a longer distance).

Finally, the deviations of the laser line by the fluid,  $x'_{\text{laser}} - x_{\text{laser}}$ , allows us to compute the flow depth,

$$D = \frac{x_{\text{laser}} - x'_{\text{laser}}}{1/\tan \phi_{\text{laser}} - 1/\tan \phi'_{\text{laser}}}, \quad (26)$$

within an accuracy  $\delta D = 0.5$  mm—slightly less than a grain diameter. According to the the Snell-Descartes law, the angle

of refraction  $\phi'_{\text{laser}}$  of the laser line reads:

$$\phi'_{\text{laser}} = \frac{\pi}{2} - \arcsin\left(\frac{1}{n} \sin\left(\frac{\pi}{2} - \phi_{\text{laser}}\right)\right), \quad (27)$$

where  $n$ , the refractive index of the water-glycerol mixture, is 1.41 at 20°C. For run 4, equation (27) yields  $\phi'_{\text{laser}} = 38.9^\circ$ .

The position of the flow surface appears noisier than that of the bed [Fig. 11(d)]. To reduce this uncertainty, we average the position of the free surface over the channel width, thus assuming it is horizontal (Fig. 3).

- [1] S. Schumm, *Annu. Rev. Earth Planet Sci.* **13**, 5 (1985).
- [2] G. Lacey, in *Minutes of the Proceedings*, Vol. 229 (Thomas Telford, London, 1930), pp. 259–292.
- [3] R. E. Glover and Q. Florey, Stable Channel Profiles, US Department of the Interior, Bureau of Reclamation, Hydraulic Laboratory Report No. Hyd-325, Washington, DC, 325 (1951).
- [4] O. Devauchelle, A. Petroff, A. Lobkovsky, and D. Rothman, *J. Fluid Mech.* **667**, 38 (2011).
- [5] G. Seizilles, O. Devauchelle, E. Lajeunesse, and F. Métivier, *Phys. Rev. E* **87**, 052204 (2013).
- [6] F. Métivier, E. Lajeunesse, and O. Devauchelle, *Earth Surf. Dynam.* **5**, 187 (2017).
- [7] G. Parker, *J. Fluid Mech.* **89**, 127 (1978).
- [8] J. D. Milliman and R. H. Meade, *J. Geol.* **91**, 1 (1983).
- [9] N. D. Smith and D. G. Smith, *Geology* **12**, 78 (1984).
- [10] F. Métivier, O. Devauchelle, H. Chauvet, E. Lajeunesse, P. Meunier, P. Ashmore, K. Blanckaert, Z. Zhang, Y. Fan, Y. Liu *et al.*, *Earth Surf. Dynam.* **4**, 273 (2016).
- [11] L. Leopold and M. Wolman, *River Channel Patterns: Braided, Meandering, and Straight* (U.S. Government Printing Office, Washington DC, 1957).
- [12] A. M. Pfeiffer, N. J. Finnegan, and J. K. Willenbring, *Proc. Natl. Acad. Sci. USA* **114**, 3346 (2017).
- [13] S. Schumm, M. Mosley, and W. Weaver, *Experimental Fluvial Geomorphology* (Wiley, New York, 1987).
- [14] C. Paola, K. Straub, D. Mohrig, and L. Reinhardt, *Earth-Sci. Rev.* **97**, 1 (2009).
- [15] M. Tal and C. Paola, *Geology* **35**, 347 (2007).
- [16] F. Métivier and L. Barrier, *Gravel-Bed Rivers: Processes, Tools, Environments* (Wiley, 2012), Chap. 34, pp. 464–473.
- [17] M. D. Reitz, D. J. Jerolmack, and J. Swenson, *Geophys. Res. Lett.* **37**, L06401 (2010).
- [18] P. Delorme, O. Devauchelle, L. Barrier, and F. Métivier, *Phys. Rev. E* **98**, 012907 (2018).
- [19] S. Ikeda, G. Parker, and Y. Kimura, *Water Resour. Res.* **24**, 713 (1998).
- [20] F. Charru, H. Mouilleron, and O. Eiff, *J. Fluid Mech.* **519**, 55 (2004).
- [21] A. Lobkovsky, A. Orpe, R. Molloy, A. Kudrolli, and D. Rothman, *J. Fluid Mech.* **605**, 47 (2008).
- [22] M. Ouriemi, P. Aussillous, and E. Guazzelli, *J. Fluid Mech.* **636**, 295 (2009).
- [23] E. Lajeunesse, L. Malverti, and F. Charru, *J. Geophys. Res.* **115**, F04001 (2010).
- [24] P. Aussillous, J. Chauchat, M. Pailha, M. Médale, and E. Guazzelli, *J. Fluid Mech.* **736**, 594 (2013).
- [25] A. S. Shields, *Mitteilung der Preussischen Versuchsanstalt für Wasserbau und Schiffbau* **26** (1936) [English translation: Application of similarity principles and turbulence research to bed-load movement (California Institute of Technology, Pasadena, CA, 1936)].
- [26] G. Parker, *J. Fluid Mech.* **89**, 109 (1978).
- [27] V. Nikora, H. Habersack, T. Huber, and I. McEwan, *Water Resour. Res.* **38**, 17 (2002).
- [28] D. Furbish, S. Fathel, M. Schmeeckle, D. Jerolmack, and R. Schumer, *Earth Surf. Process. Landforms* **42**, 214 (2017).
- [29] G. Seizilles, E. Lajeunesse, O. Devauchelle, and M. Bak, *Phys. Fluids* **26**, 013302 (2014).
- [30] A. Abramian, O. Devauchelle, G. Seizilles, and E. Lajeunesse, *Phys. Rev. Lett.* **123**, 014501 (2019).
- [31] See Supplemental Material at <http://link.aps.org/supplemental/10.1103/PhysRevE.102.053101> for the data and the bedload movie.
- [32] J. Stebbings, *Proc. Inst. Civil Eng.* **25**, 485 (1963).
- [33] G. Parker, *J. Fluid Mech.* **76**, 457 (1976).
- [34] A. Abramian, O. Devauchelle, and E. Lajeunesse, *J. Fluid Mech.* **863**, 601 (2019).
- [35] A. Abramian, Self organisation of sediment transport in alluvial rivers, Université Sorbonne Paris Cité, 2018, English (NNT : 2018USPCC202).
- [36] P. Bak, C. Tang, and K. Wiesenfeld, *Phys. Rev. A* **38**, 364 (1988).
- [37] F. M. Henderson, *J. Hydraul. Div. ASCE* **87**, 109 (1961).
- [38] C. Phillips and D. Jerolmack, *Science* **352**, 694 (2016).